Multibeam Antenna for *Ka*-Band CubeSat Connectivity Using 3-D Printed Lens and Antenna Array

Kamil Trzebiatowski, Weronika Kalista, Mateusz Rzymowski, *Member, IEEE*, Łukasz Kulas, *Senior Member, IEEE*, and Krzysztof Nyka, *Senior Member, IEEE*

***Abstract*—In this letter, the design of a passive multibeam lens antenna is proposed for the CubeSat space communication system as an alternative application of a 2-D microstrip antenna array that has originally been designed for a 39-GHz 5G multi-user, multiple-input, multiple-output (MU-MIMO) system. The half-ellipsoid lens is 3-D printed using stereolithography technology. The antenna prototype is capable of selecting the main beam between 16 different directions with a gain ranging from 14 to 16 dBi and a half-power beamwidth of 14°–18°. The measurements carried out in an anechoic chamber show good agreement with numerical simulations. The presented prototype shows that by employing 3-D printing technologies existing antennas can be easily and inexpensively converted to switched-beam or multibeam solutions.**

***Index Terms*—3-D printing, additive manufacturing, CubeSat, fifth-generation (5G) communication, Internet-of-Things, millimeter-wave antenna, passive multibeam antennas, reconfigurable antennas, switched-beam antennas.**

I. Introduction

DURING recent years, the exploitation of space in the low Earth orbit has grown rapidly, mainly through a large number of small satellites [1], [2]. These satellites require reliable and high-throughput intersatellite and ground-to-satellite communication networks. To achieve this, the Internet-of-Space-Things (IoST) system has been proposed as a space extension of the Internet-of-Things (IoT) paradigm. The main components of IoST networks are ground stations, unmanned aerial vehicles, and small satellites called CubeSats [1]–[3], which are used to create satellite constellations.

Manuscript received 30 March 2022; revised 10 May 2022 and 28 June 2022; accepted 5 July 2022. Date of publication 7 July 2022; date of current version 28 October 2022. This work was supported by the Gdansk University of Technology through the DEC-3/2020/IDUB/III.4.3/Pu Grant under the PLUTONIUM—"Excellence Initiative—Research University" Program. *(Corresponding author: Kamil Trzebiatowski.)*

Kamil Trzebiatowski, Weronika Kalista, Mateusz Rzymowski, and Krzysztof Nyka are with the Department of Microwave and Antenna Engineering, Faculty of Electronics, Telecommunications and Informatics, Gdansk University of Technology, 80-233 Gdansk, Poland (e-mail: kamil.trzebiatowski@pg.edu.pl; weronika.kalista@pg.edu.pl; mateusz.rzymowski@pg.edu.pl; krzysztof.nyka@pg.edu.pl).

Łukasz Kulas is with the Department of Microwave and Antenna Engineering, Faculty of Electronics, Telecommunications and Informatics, Gdansk University of Technology, 80-233 Gdansk, Poland, and also with the Digital Technologies Center, Gdansk University of Technology, 80-233 Gdansk, Poland (e-mail: lukasz.kulas@eti.pg.gda.pl).

Digital Object Identifier 10.1109/LAWP.2022.3189073

The wireless communication in the IoST can be realized in a wide spectrum, ranging from *L*-band (1–2 GHz), through *X*-band (8–12 GHz), up to *Ka*-band (26.5–40 GHz) [1]. The key components of wireless networks are antennas, which should provide the best possible performance preserving the smallest possible dimensions as the available space inside satellites is limited [4]–[6]. In the millimeter-wave bands, high-gain antennas are often needed. Usually requiring a large aperture, they are difficult or impossible to realize within the CubeSats' size constraints. Alternatively, a low-gain antenna element can be coupled with a dielectric lens, thus increasing the gain without an excessive growth of the physical aperture [11]. Adding a lens can also turn an antenna comprising a set of separately fed radiators into a multibeam or switched-beam antenna. Such antennas provide beam diversity that is often preferred in various IoST scenarios to improve connectivity. In the context of CubeSats, passive multibeam antennas [7] and single-input reconfigurable antennas, such as switched-beam antennas [8]–[10], are particularly interesting. Although they usually provide less flexibility than digital beamforming solutions, they have lower complexity and energy consumption.

In the literature, several examples of lens-based switched-beam and multibeam antennas can be found [11]–[21]. The typical design consists of an antenna (or an array of planarly distributed antennas) placed behind a dielectric lens [11]–[18]. In [11], the general lens-based multibeam antenna and its implementation were presented. The beam direction can be deflected by changing the active radiating microstrip patch. Similar designs with added switched feeding networks are investigated in [12] and [13]. Designs in [19]–[21] show a similar approach to realizing switched-beam or multibeam antennas, where multiple antenna radiators are placed around a single lens. Each radiator is aligned with one of the lens' axes of symmetry and the beams are focused in those directions. This approach provides wider scanning angles than by placing radiators in one plane. A disadvantage of these solutions is that they are usually very large compared to the wavelength and would be difficult to fit into a small satellite.

The dielectric lens used in the switched-beam antenna designs can have ellipsoidal [11], [18], hemispherical [12]–[14], circular [19], [21], or even flat shapes [15]–[17]. Regardless of the shape, which can be chosen arbitrarily, the lens is usually optimized to maximize the gain or angular coverage of aggregated antenna beams. The antenna lenses can be quickly and affordably manufactured in 3-D printing technology, such as stereolithography (SLA) or fuse deposition modeling (FDM) [14], [17], [22]–[26].

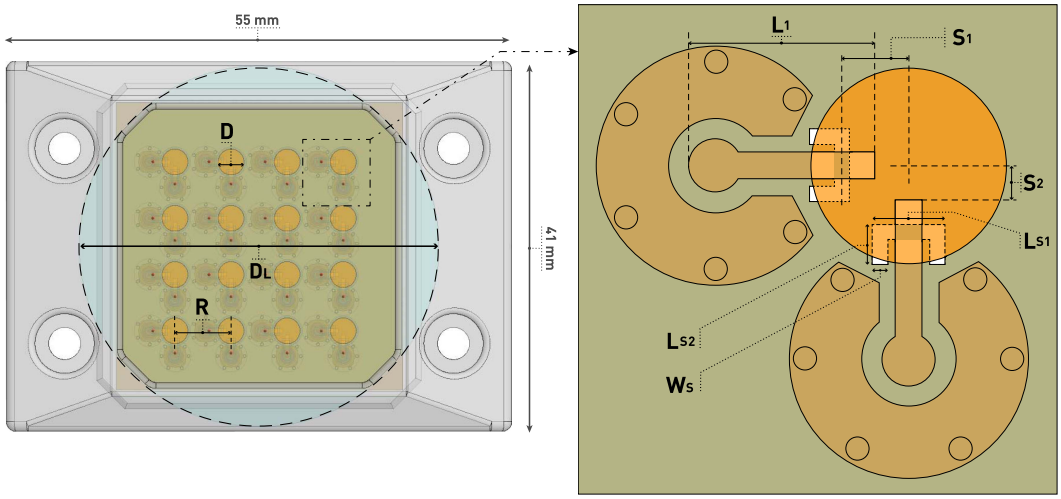

Fig. 1. Design of a multiport dual-polarized antenna array with a holder—overall top view (left) and a single-antenna element with solder pads for SMPS connectors (right). Lens outline (diameter D_L) is in light blue.

In this letter, we propose a new approach different from the state-of-the-art designs, which optimize the system of radiators together with the lens to create an integrated switched-beam or multibeam antenna. In our work, an existing antenna array, designed, optimized, and fabricated for a standalone application in fifth-generation (5G) multi-user, multiple-input, multiple-output (MU-MIMO) systems, is adapted to create a passive multibeam antenna intended for space applications by coupling it with a 3-D printed dielectric lens. Alternatively, the proposed antenna can be used for beam switching operation if an appropriate switching circuit is added. In the letter, we describe the employed antenna array, present the design and fabrication of the lens, and discuss measurement results comparing them with the numerical simulations. The presented modular approach, which is the novelty of this work, could be employed for any multiport planar antenna array designed for another mode of operation, such as digital or analog beamforming, particularly intended for intersatellite communication. It is especially beneficial in CubeSats, where lightweight printed lenses can be inexpensively customized to match particular mission communication scenarios without changing the radiator array and feeding network.

TABLE I
DIMENSIONS OF THE ANTENNA, IN mm

D	W_s	L_{s1}	L_{s2}	S_1	S_2
2.6	0.2	0.974	0.535	0.9	0.45
L_1	R	D_L	H_L	S_L	A_L
2.15	5.77	37.0	16.5	5.5	30.96

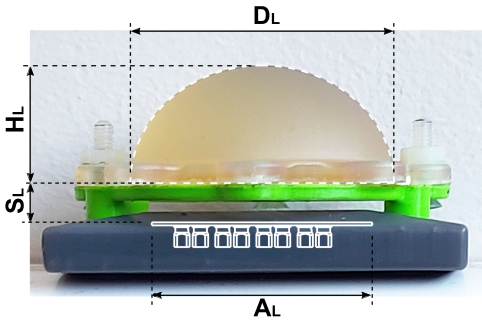

Fig. 2. Side view of the antenna array with the lens. The array PCB and SMPS connectors are drawn as they are hidden within the holder.

II. ANTENNA DESIGN

The proposed antenna design utilizes a previously realized and measured multiport linearly dual-polarized microstrip array [27], presented in Fig. 1. In this letter, only the horizontal polarization is investigated. The array is formed by 16 elements, each consisting of a radiating patch and feeding network. The microstrip patches are placed with a spacing R between their centers, which is constrained by connector size and a diameter of a single patch. The R value was chosen as 0.75 λ_0, where λ_0 is free space wavelength at the resonant frequency (39 GHz). The design uses a two-layered substrate with patches on the top layer (CuClad217 substrate with 0.254 mm thickness) and a feeding network on the bottom layer (RT/duroid 5880 substrate with 0.127 mm thickness).

A circular microstrip patch of diameter D is chosen as a radiating element due to its symmetry required for dual-polarized operation [28], [29]. The patch, as shown in Fig. 1, is fed through two orthogonal C-shaped slots in the ground plane. The slots are defined by three parameters: width W_s, lengths L_{s1}, L_{s2}, and are placed with a distance S_1 from the patch center. The antenna is fed through sub-miniature push-on, sub-micro (SMPS) connectors soldered to feeding microstrip lines on the bottom layer. They have a length of L_1 and are placed with an offset of S_2 from the patch center. The numerical values of the dimensions are presented in Table I.

The array was adapted to a design of multibeam antenna by adding a homogeneous all-dielectric half-ellipsoid shaped lens, providing both beam deflection and gain enhancement. 2-D beam selection of the antenna is realized by exciting ports of single patches selectively. This allows for an alternative beam-switching operation by using an optional switching circuit connected to the SMPS ports. Deflection of 16 separate beams is possible due to the diversity of patch positions relative to the axis of the lens. A side view of the antenna with the array printed circuit board (PCB) and SMPS connectors is presented in Fig. 2.

The lens was optimized by changing its dimensions (D_L, H_L, S_L) for fixed $\varepsilon_r = 2.66$. The goal consisted of three criteria

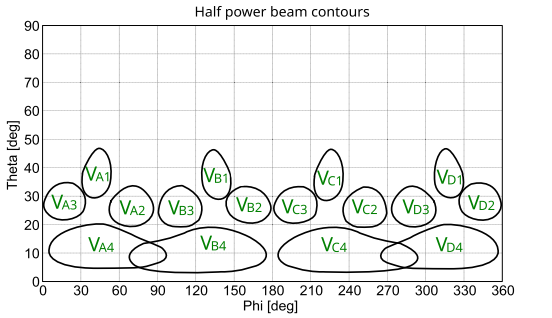

(a)

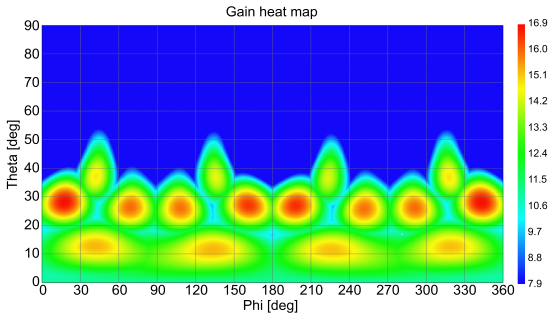

(b)

Fig. 3. Simulated gain at 39 GHz for all possible beams. (a) Half-power gain contours. (b) Aggregated gain heat map (dBi).

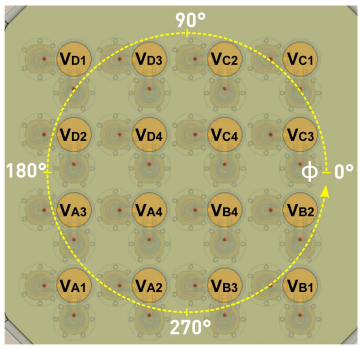

Fig. 4. Antenna elements corresponding to the beams shown in Fig. 3(a).

regarding beam shaping: 1) scan loss lower than 3 dB, 2) 360° coverage in the horizontal plane (variable ϕ) for a given θ, and 3) beams wide enough to provide continuous coverage with gain variation less than 6 dB. Dimensions of the designed lens are as follows: Diameter $D_L = 37$ mm, which corresponds to $4.8\lambda_0$ at 39 GHz, height $H_L = 16.5$ mm, and the spacing $S_L = 5.5$ mm. The air gap prevents severe degradation of the antenna matching and has an impact on the main beam direction. Using a lens with larger diameter increases antenna gain, but at the same time limits beam deflection angle. The maximum antenna radiator to lens center offset is 8.7 mm in both array axes.

The gain plots of all 16 beams obtained from simulations performed using Altair Feko 2021.2 software are shown in Fig. 3(a) and (b). Fig. 3(a) shows half-power gain coverage relative to the maximum gain for each beam. The beams are denoted by the symbols of corresponding excited patch radiators introduced in Fig. 4. An aggregated gain plot as a heat map

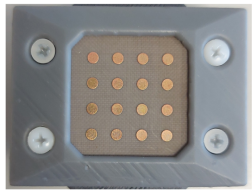

(a)

(b)

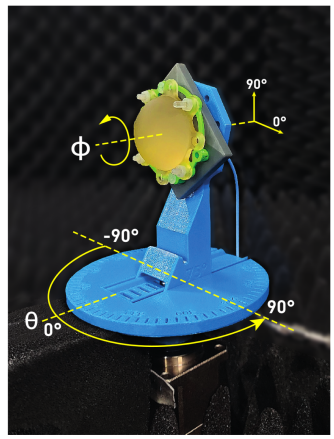

(c)

Fig. 5. Fabricated antenna. (a) Array top view. (b) Array bottom view. (c) Array with a lens mounted on a turntable in an anechoic chamber.

with a maximum value equal to the common maximum gain of all beams $G_{\max} = 16.9$ dBi (for beam V_{A3}) is in Fig. 3(b). The maximum simulated gain of individual beams ranges from 14.3 dBi to $G_{\max}$, whereas the maximum gain of a single-patch radiator is 7.4 dBi. The plot shows that the antenna provides continuous coverage in the whole 360° range for ϕ and 0°–33° range for θ with the gain variation of mostly less than 5.2 dB. There are only a few very narrow spots where the gain falls from $G_{\max}$ by 7.5 dB. From this plot, one can also read the directions of the beams and choose the angular cross-sections for corresponding radiation pattern measurements. Simulated antenna efficiency ranges from 48% to 53% and sidelobe level (SLL) in maximum gain cross-section ranges from -19.2 to -14.3 dB.

III. Fabrication and Measurements

The designed antenna array was manufactured in a standard multilayer PCB technology and its top and bottom view with 3-D printed holder are presented in Fig. 5(a) and (b), respectively. The lens was fabricated using 3-D printing SLA technology, which is more precise compared to simpler 3-D printing methods such as FDM. FormLabs High Temp resin with dielectric properties reported in [31] is equal to $\varepsilon_r = 2.66$ and $\tan\delta = 0.03$ was used as a dielectric material. Being durable and having a low density of 1.28 g/cm^3, it is a competitive material to silicon glass used in [12] concerning the lens weight, which is relevant in space applications, particularly in CubeSats. The weight of the fabricated lens is 15.2 g. The fabricated prototype of the antenna is shown in Fig. 2. The lens is mounted at a fixed distance from the array PCB using a 3-D printed spacer (a green structure in Fig. 2).

All measurements were conducted using a measurement setup consisting of an anechoic chamber, an R&S ZVA50 network analyzer, a transmitting antenna, and an antenna under test in receiving mode, held by a stand placed on a turntable. Radiation patterns in the elevation plane are measured in the range of θ from $-80°$ to 80° with a resolution of 2°. Because the antenna array is uniform and symmetrical, only radiation patterns for a group of four representative radiating patches ($V_{D1} - V_{D4}$) were measured while the rest can be approximated by mirroring. The vertical cuts were set individually for each beam at ϕ angles of

TABLE II
MEASURED PARAMETERS OF BEAMS V_{Dn}

Beam symbol	Bare patch	V_{D1}	V_{D2}	V_{D3}	V_{D4}
Main lobe θ direction [°]	0	40	30	26	14
HPBW [°]	31.8	17.6	14.0	16.9	17.8
SLL [dB]	-14.6	-9.4	-10.6	-10.2	-19.2
Gain [dBi]	6.5	14.7	15.8	15.1	14.5

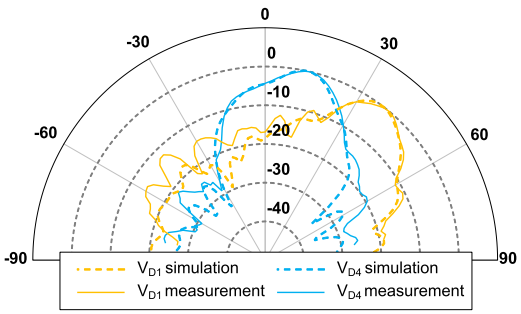

(a)

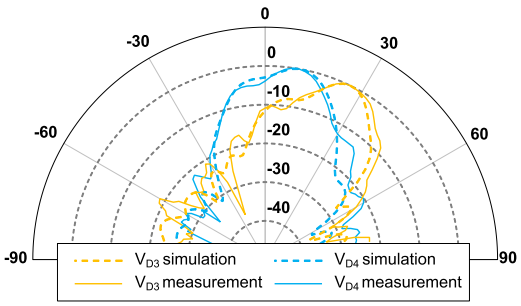

(b)

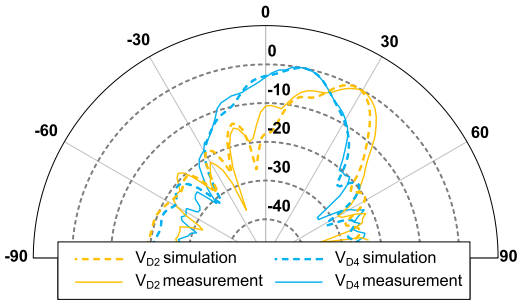

(c)

Fig. 6. Simulated and measured normalized radiation patterns (dB) at 39 GHz in vertical plane (θ) in cuts at fixed angles. (a) $\phi = 315°$. (b) $\phi = 290°$. (c) $\phi = 345°$.

their maximum gain: V_{D1} in $\phi = 315°$, V_{D2} in $\phi = 345°$, V_{D3} in $\phi = 290°$, and V_{D4} in $\phi = 315°$. Because of its broad beam, V_{D4} was also measured at $\phi = 290°$ and 345° for comparison with V_{D1} and V_{D2}. Fig. 5(c) presents the prototype in the anechoic chamber with marked directions of rotation for θ and ϕ angles.

The measurement results for beams V_{Dn} are summarized in Table II. The simulated and measured normalized radiation patterns in the vertical cuts are compared in Fig. 6(a)–(c), and it can be noticed that they agree very well. The main lobe direction for all excited patches differs at a maximum of 2° from

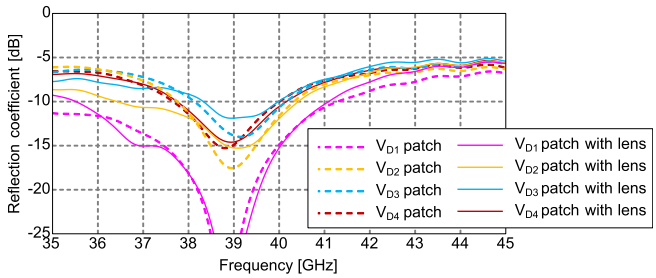

Fig. 7. Measured reflection coefficient of patches $V_{D1} - V_{D4}$ with and without the lens.

simulation results. The most significant discrepancy is in SLL, which in the worst case increases from simulated −18 dB to measured −10.2 dB. The measured gain is equal to 6.5 dBi for the bare patch and in the range of 14.5–15.8 dBi for single beams (V_{D1}–V_{D4}) with the lens. The 3 dB gain bandwidth is 12.3%. The average simulated dielectric loss in the lens is 2.3 dB at 39 GHz, which results in total simulated efficiency of 47% to 54% for the beams V_{D1} to V_{D4}. In effect, calculated directivity is 17.8–18.4 dBi, which corresponds to aperture efficiency of 26.2%–30.8%.

The measured values of the reflection coefficient for beams V_{Dn} are shown in Fig. 7. There is only a small deterioration of the reflection coefficient caused by the lens so no further matching improvement is required. The −10 dB matching bandwidth for the worst case (V_{D3}) is 38.3–40 GHz.

IV. CONCLUSION

In this letter, we present a design and experimental verification of a millimeter-wave multibeam lens antenna that directly adapts a separately designed multiport patch array by adding a 3-D printed lens. The antenna produces separate beams in 16 different directions and can be extended to provide a switched-beam operation. One of the advantages of the designed lens is that no additional optimization of the array is required because the designed lens has a minor influence on the antenna matching. Due to its small physical aperture and weight, the antenna is suitable for the IoST applications, such as intersatellite communication in CubeSat constellations. Another advantage of the proposed modular approach to designing lens-based multibeam antennas is that they can be customized for specific missions by replacing only inexpensive printed lenses.

ACKNOWLEDGMENT

This letter is a result of the BEYOND5 (www.beyond5.eu) project, which has received funding from the ECSEL Joint Undertaking (JU) under Grant 876124. The JU receives support from the European Union's Horizon 2020 research and innovation programme and from France, Germany, Turkey, Sweden, Belgium, Poland, Netherland, Israel, Switzerland, and Romania. The document reflects only the authors' view and the Commission is not responsible for any use that may be made of the information it contains.

REFERENCES

[1] I. F. Akyildiz, A. Kak, and S. Nie, "6G and beyond: The future of wireless communications systems," *IEEE Access*, vol. 8, pp. 133995–134030, 2020.

[2] Y. Rahmat-Samii, V. Manohar, and J. M. Kovitz, "For satellites, think small, dream big: A review of recent antenna developments for CubeSats," *IEEE Antennas Propag. Mag.*, vol. 59, no. 2, pp. 22–30, Apr. 2017.

[3] M. N. Sweeting, "Modern small satellites - Changing the economics of space," *Proc. IEEE*, vol. 106, no. 3, pp. 343–361, Mar. 2018.

[4] S. Gao, Y. Rahmat-Samii, R. E. Hodges, and X. Yang, "Advanced antennas for small satellites," *Proc. IEEE*, vol. 106, no. 3, pp. 391–403, Mar. 2018.

[5] L. Leszkowska, M. Rzymowski, K. Nyka, and L. Kulas, "High-gain compact circularly polarized X-band superstrate antenna for CubeSat applications," *IEEE Antennas Wireless Propag. Lett.*, vol. 20, no. 11, pp. 2090–2094, Nov. 2021.

[6] L. Leszkowska, M. Rzymowski, K. Nyka, and L. Kulas, "High gain circularly polarized antenna with a superstrate layer for aerospace communication," presented at the Small Satell. Syst. Serv. Symp., 2022, Accessed: Jul. 19, 2022. [Online]. Available: https://az659834.vo.msecnd.net/eventsairwesteuprod/production-atpi-public/f51e796fa2604523954015f3bcca45a7

[7] W. Hong et al., "Multibeam antenna technologies for 5G wireless communications," *IEEE Trans. Antennas Propag.*, vol. 65, no. 12, pp. 6231–6249, Dec. 2017.

[8] K. Trzebiatowski, M. Rzymowski, L. Kulas, and K. Nyka, "Simple 60 GHz switched beam antenna for 5G millimeter-wave applications," *IEEE Antennas Wireless Propag. Lett.*, vol. 20, no. 1, pp. 38–42, Jan. 2021.

[9] L. Leszkowska, D. Duraj, M. Rzymowski, K. Nyka, and L. Kulas, "Electronically reconfigurable superstrate (ERES) antenna," in *Proc. 13th Eur. Conf. Antennas Propag*., 2019, pp. 1–4.

[10] G. Jin, M. Li, D. Liu, and G. Zeng, "A simple four-beam reconfigurable antenna based on monopole," *IEEE Access*, vol. 6, pp. 30309–30316, 2018.

[11] X. Wu, G. V. Eleftheriades, and T. E. van Deventer-Perkins, "Design and characterization of single- and multiple-beam mm-wave circularly polarized substrate lens antennas for wireless communications," *IEEE Trans. Microw. Theory Techn.*, vol. 49, no. 3, pp. 431–441, Mar. 2001.

[12] A. Artemenko, A. Maltsev, A. Mozharovskiy, A. Sevastyanov, V. Ssorin, and R. Maslennikov, "Millimeter-wave electronically steerable integrated lens antennas for WLAN/WPAN applications," *IEEE Trans. Antennas Propag.*, vol. 61, no. 4, pp. 1665–1671, Apr. 2013.

[13] A. Artemenko, A. Mozharovskiy, A. Maltsev, R. Maslennikov, A. Sevastyanov, and V. Ssorin, "Experimental characterization of E-band two-dimensional electronically beam-steerable integrated lens antennas," *IEEE Antennas Wireless Propag. Lett.*, vol. 12, pp. 1188–1191, 2013.

[14] C. Ballesteros, M. Maestre, M. C. Santos, J. Romeu, and L. Jofre, "A 3D printed lens antenna for 5G applications," in *Proc. IEEE Int. Symp. Antennas Propag. USNC-URSI Radio Sci. Meeting*, 2019, pp. 1985–1986.

[15] M. Imbert, A. Papió, F. De Flaviis, L. Jofre, and J. Romeu, "Design and performance evaluation of a dielectric flat lens antenna for millimeter-wave applications," *IEEE Antennas Wireless Propag. Lett.*, vol. 14, pp. 342–345, 2015.

[16] M. Imbert, J. Romeu, M. Baquero-Escudero, M. Martinez-Ingles, J. Molina-Garcia-Pardo, and L. Jofre, "Assessment of LTCC-based dielectric flat lens antennas and switched-beam arrays for future 5G millimeter-wave communication systems," *IEEE Trans. Antennas Propag.*, vol. 65, no. 12, pp. 6453–6473, Dec. 2017.

[17] E. Garcia-Marin, D. S. Filipovic, J. L. Masa-Campos, and P. Sanchez-Olivares, "Ka-band multi-beam planar lens antenna for 5G applications," in *Proc. 14th Eur. Conf. Antennas Propag.*, 2020, pp. 1–5.

[18] J. Ala-Laurinaho et al., "2-D beam-steerable integrated lens antenna system for 5G E-band access and backhaul," *IEEE Trans. Microw. Theory Techn.*, vol. 64, no. 7, pp. 2244–2255, Jul. 2016.

[19] B. Schoenlinner, X. Wu, J. P. Ebling, G. V. Eleftheriades, and G. M. Rebeiz, "Wide-scan spherical-lens antennas for automotive radars," *IEEE Trans. Microw. Theory Techn.*, vol. 50, no. 9, pp. 2166–2175, Sep. 2002.

[20] A. E. I. Lamminen et al., "Beam-switching dual-spherical lens antenna with low scan loss at 71–76 GHz," *IEEE Antennas Wireless Propag. Lett.*, vol. 17, no. 10, pp. 1871–1875, Oct. 2018.

[21] P.-Y. Feng, S.-W. Qu, and S. Yang, "Defocused cylindrical Luneburg lens antennas with phased array antenna feed," *IEEE Trans. Antennas Propag.*, vol. 67, no. 9, pp. 6008–6016, Sep. 2019.

[22] H. Yi, S. Qu, K. Ng, C. H. Chan, and X. Bai, "3-D printed millimeter-wave and terahertz lenses with fixed and frequency scanned beam," *IEEE Trans. Antennas Propag.*, vol. 64, no. 2, pp. 442–449, Feb. 2016.

[23] K. X. Wang and H. Wong, "Design of a wideband circularly polarized millimeter-wave antenna with an extended hemispherical lens," *IEEE Trans. Antennas Propag.*, vol. 66, no. 8, pp. 4303–4308, Aug. 2018.

[24] W. Shao and Q. Chen, "2-D beam-steerable generalized Mikaelian lens with unique flat-shape characteristic," *IEEE Antennas Wireless Propag. Lett.*, vol. 20, no. 10, pp. 2033–2037, Oct. 2021.

[25] H. Giddens, A. S. Andy, and Y. Hao, "Multimaterial 3-D printed compressed Luneburg lens for mm-wave beam steering," *IEEE Antennas Wireless Propag. Lett.*, vol. 20, no. 11, pp. 2166–2170, Nov. 2021.

[26] A. Papathanasopoulos, J. Budhu, Y. Rahmat-Samii, R. E. Hodges, and D. F. Ruffatto, "3D-printed shaped and material-optimized lenses for next-generation spaceborne wind scatterometer weather radars," *IEEE Trans. Antennas Propag*., vol. 70, no. 5, pp. 3163–3172, May 2022.

[27] K. Trzebiatowski, J. Fromme, D. Duraj, L. Kulas, and K. Nyka, "A dual-polarized 39 GHz 4x4 microstrip antenna array for 5G MU-MIMO airflight cabin connectivity," 2022, submitted for publication.

[28] T. H. Jang, H. Y. Kim, D. M. Kang, S. H. Kim, and C. S. Park, "60 GHz low-profile, wideband dual-polarized U-slot coupled patch antenna with high isolation," *IEEE Trans. Antennas Propag.*, vol. 67, no. 7, pp. 4459–4462, Jul. 2019.

[29] X. Yang et al., "Broadband dual-polarized phased array with broadside and endfire radiation for 5G millimeter wave communications," in *Proc. Comput. Commun. IoT Appl.*, 2019, pp. 210–212.

[30] L. Catarinucci, S. Guglielmi, R. Colella, and L. Tarricone, "Compact switched-beam antennas enabling novel power-efficient wireless sensor networks," *IEEE Sensors J.*, vol. 14, no. 9, pp. 3252–3259, Sep. 2014.

[31] G. B. Wu, Y. S. Zeng, K. F. Chan, S. W. Qu, and C. H. Chan, "3-D printed terahertz lens with circularly polarized focused near field," in *Proc. 13th Eur. Conf. Antennas Propag.*, 2019, pp. 1–4.